Available online at www.sciencedirect.com
ScienceDirect
Powder Technology 181 (2008) 195–204
POWDER TECHNOLOGY
www.elsevier.com/locate/powtec

An extended radioactive particle tracking method for systems with irregular moving boundaries

Jocelyn Doucet, François Bertrand *, Jamal Chaouki *

Department of Chemical Engineering, École Polytechnique de Montreal, P.O. Box 6079, Station Centre-Ville, Montreal, Quebec, Canada H3C 3A7

Received 16 May 2006
Available online 23 December 2006

Abstract

The aim of this paper is to present an extension of the original non-intrusive radioactive particle tracking method (RPT) to any geometries with irregular moving boundaries. The principal advantage of RPT over other non-intrusive methods is that it enables the visualization of rather large systems. However, the underlying reconstruction algorithm is limited to cylindrically shaped systems such as fluidized beds and columns. It excludes a wide variety of systems involving multiphase flows such as, for instance, spherical reactors, cyclones and powder silos, hoppers and blenders, all of which are thus currently out of reach of current RPT capabilities. This work addresses these limitations and proposes an approach that solves the inverse map problem to reconstruct the tracer position with time by using a mesh of unstructured cells to discretize the system geometry and kinematics. The anisotropy induced by the gas–solid interface is discussed and taken into account in the proposed model. To show the possibilities and assess the performance of the developed technique, the flow of particles in a 16-qt V-blender is mapped and the mean velocity field is computed.

Keywords: Radioactive particle tracking; Non-intrusive methods; Solid mixing; V-blender; Pharmaceutical processes; Monte-Carlo methods

1. Introduction

1.1. Background

The motion of solid particles plays an important role in the dynamics of mixing. For this reason, an appropriate knowledge of the particle dynamics leads to a better understanding of the mixing mechanisms involved and, ultimately, helps in improving the design of existing installations. In the last few years, several works have addressed the development of sophisticated deterministic models for the flow behavior of particles, based for instance on the discrete element method (DEM) [1]. However, few experimental investigations have mapped the entire flow because of the relative complexity of the operation. In fact, it is difficult to measure the flow field without interfering with the matter and affecting the measure itself, as experienced in the case of thief sampling [2].

To address this main limitation, several non-intrusive velocimetric methods have been developed, which map the flow field of one phase by tracking the motion of a single tracer particle in this studied phase. The opaque nature of a particulate solid as well as the relative complexity of blenders rules out any of the conventional velocimetric techniques, such as Laser Doppler Anemometry (LDA), Particle Image Velocimetry (PIV), fluorescent PIV and cinematography, which have been mainly applied for surface flows and hopper discharges [3]. This is why new methods based on radioactive measurements have been developed in order to obtain quantitative information about the exact location of the tracer in the domain. Two major methods are currently employed in the literature. The first one, based on positron annihilation (Positron Emission Particle Tracking or PEPT), was developed by Hawksworth et al. [4]. The second one, which is the topic of this work, uses a tracer with isotropic gamma-ray emission that comes from a particle containing irradiated Sc^{46}. This technique is known as

* Corresponding authors.
E-mail addresses: francois.bertrand@polymtl.ca (F. Bertrand), jamal.chaouki@polymtl.ca (J. Chaouki).

0032-5910/$ - see front matter © 2006 Elsevier B.V. All rights reserved.
doi:10.1016/j.powtec.2006.12.019

radioactive particle tracking (RPT), originally proposed by Lin et al. [5]. The major difference between these techniques lies in the varying nature of the radiations measured, which yields to the use of different detection systems. Several works have shown the capabilities of RPT for monitoring the granular motion of particulate solids in spouted and circulating fluidized beds, principally by the groups of Dudukovic [6,7] and Chaouki [8–11]. A typical experimental setup for the application of RPT to multiphase reactors is presented in Fig. 1.

1.2. Motivation

The use of nuclear velocimetric methods for investigating solid mixing in industrial blenders is relatively new and most of the studies have been performed using principally PEPT, following the original work of Bridgwater et al. [12]. As a matter of fact, the last decade has been particularly productive for generating experimental data with PEPT for different types of mixers, such as the ploughshare [13–15], the planetary [16], the single blade [17] and the high shear [18]. Recent works have also successfully applied this technique to obtain the flow field in a V-blender for different fill levels [19]. In the case of RPT, the detection system consists of an array of 8 to 16 Sodium Iodide (NaI-Tl) detectors that record the number of disintegration events coming from the source within the domain during a specific dwell time (typically 5 to 10 ms). This setup has the main advantage of being relatively compact and cheap in comparison to the previous method. It also enables the study of a system with rather large dimensions since the detectors can be positioned individually around the system. This is why most of the literature referring to this method is principally oriented to the study of rather large and tall multiphase reactors [20,21,7].

In the last few years, several works have been performed in order to improve RPT resolution and sensitivity either by improving the design of the experiments [22] or by selecting the appropriate isotope for the tracer [23,22]. So far, the reconstruction of the tracer position by using the measurements obtained from the detectors (referred to as the inverse map problem) has been achieved exactly in the case of cylindrically shaped domains by accounting for the geometrical anisotropy induced by the boundaries, following the original work of Larachi et al. [24,8]. This anisotropy as well as the solid angle with each detector must be well accounted for since the quality of the map depends essentially on the level of precision with which one can predict these two quantities. In the case of irregular geometries (i.e., with no analytical expressions to represent the boundaries) submitted to unknown kinematics, no work has been done on the solution of the inverse map problem. This limits, unfortunately, the range of applications of this powerful method to only a few families of chemical reactors and vessels. In the case of powder mixing systems, this constitutes a major limitation as evidenced by one single report on this topic, which involved rotary kilns [25].

Most of the blenders used in industry are of complex manufacture, such as the V-blender and a variety of tote blenders, which are out of reach of RPT techniques for experimental investigation. Moreover, such systems generally exhibit kinematics for which RPT is still unadapted. An easy way around this limitation would be to have an array of detectors moving in the Lagrangian framework with the blender. Unfortunately, from a mechanical standpoint, this solution is hardly feasible and the sensitivity of the detectors to vibrations would deteriorate the quality of the data.

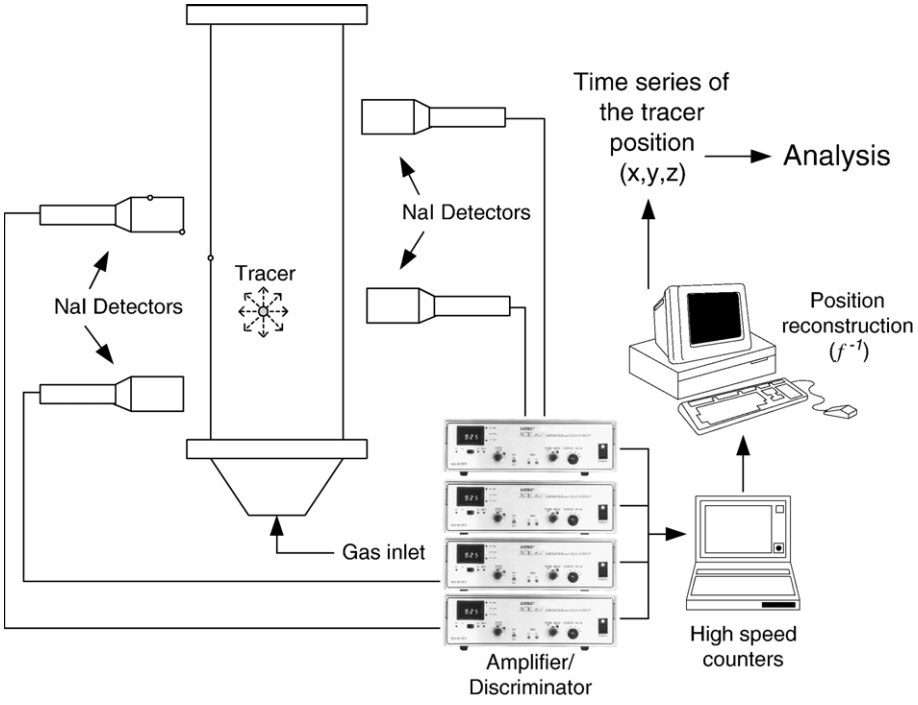

Fig. 1. Original application of RPT to the study of multiphase reactors. The method enables the visualization of the flow field in various types of opaque systems.

The aim of this paper is to present an extended RPT technique that is suitable for domains with irregular moving boundaries. This level of flexibility is required to study the granular flow in a broad range of blenders that are currently unreachable with the existing RPT technique. The method will first be described in detail. It will then be applied to a 16-qt Patterson–Kelley V-blender with monosized 3-mm glass beads, to validate it and to show the great amount of information that can be generated to elucidate the dynamics of mixing in such complex systems of industrial relevance.

2. Method

2.1. The RPT algorithm

The RPT algorithm maps a set of γ disintegration events that come from a tracer containing an irradiated isotope, to a spatial position $\mathbf{x}(x, y, z)$ in a domain $V \subset \mathbb{R}^3$ with its boundary ∂V. The set of events recorded $\Phi = \{\Phi_i\}_{i=1..N}$ by each of the N detectors depends on the position of the tracer at time t. The latest generation of RPT methods reconstructs the position of the tracer by solving a minimization problem between measured events and a rigorous phenomenological model proposed by Beam et al. [26] and thereafter applied by Larachi et al. [24]. This model relates the position of the emitter to the number of events recorded by each detector surrounding the system. A typical setup for an RPT experiment is presented in Fig. 1. The detectors measure different levels of radiation depending on the position of the emitter. By using an appropriate model, the exact location of the tracer can then be obtained. As it has been largely discussed, the inverse function that makes up this model is complex, but can be evaluated rigorously by means of a Monte-Carlo method. This approach is the topic of the next section.

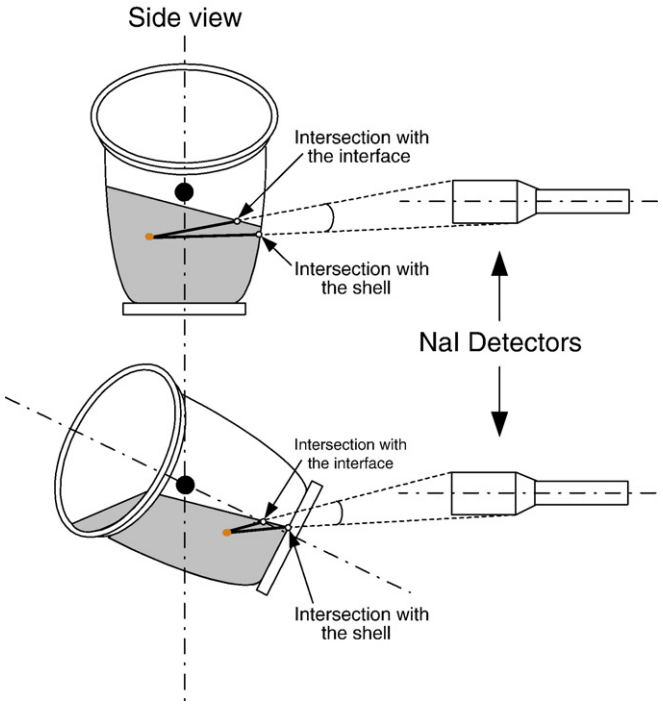

Fig. 2. Illustration of the V-blender setup for the study. Depending on the position of the blender, the ray path may cross the interface or the shell.

2.2. The phenomenological model

The location of the tracer is represented in cartesian coordinates by $\mathbf{x}(x,y,z) \in V$, which is a smooth map $f^{-1}: \mathbb{R}^{N+1} \mapsto V$ such that $f^{-1}(\Phi_1, \Phi_2 \ldots \Phi_N, t) = \mathbf{x}(t)$. The function that relates the number of counts measured by detector i to the location of the tracer in the domain is given by [27]:

$$\Phi_i(x,t) = \frac{T v R \phi \xi_i(\mathbf{x},t)}{1 + \tau v R \phi \xi_i(\mathbf{x},t)}, \tag{1}$$

which is the expected number of events that should be recorded at position x at time t. In this expression, T is the dwell time, τ is the dead-time of the detectors, R is the source activity, v is the number of photons emitted by disintegration, ϕ is the photopeak-to-total ratio, and $\xi_i(\mathbf{x}, t)$ is the efficiency of detector i with respect to a given position $\mathbf{x}$. In our case, since the boundaries of the domain vary with time according to known kinematics, this efficiency becomes time dependent.

2.3. Computation of the efficiency

The whole challenge in the proposed method is the exact computation of the efficiency term $\xi_i(\mathbf{x},t)$ in Eq. (1). By definition, the efficiency is related to the following surface integral:

$$\xi_i(\mathbf{x},t) = \oiint_{\Omega} \rho_d(\mathbf{r},t)\rho_s(\mathbf{r},t)\left(\frac{\mathbf{r}\cdot d\mathbf{A}}{\|\mathbf{r}\|^3}\right), \tag{2}$$

where $\mathbf{r}$ is the direction vector from a given position $\mathbf{x}$ to a point on the surface of the detector, $d\mathbf{A}$, the external surface vector normal to the surface at the contact point on the detector crystal and Ω, the solid angle. The functions $\rho_d(\mathbf{r}, t)$ and $\rho_s(\mathbf{r}, t)$ are the probability of interaction functions for the detector and the solid phase, respectively, as given by the Beer–Lambert equations:

$$\int_0^{\sigma(t)} -\mu_d(s)ds = \ln[1 - \rho_d(\mathbf{r},t)], \tag{3}$$

$$\int_0^{\ell(t)} -\mu_s(s)ds = \ln[\rho_s(\mathbf{r},t)], \tag{4}$$

where $\sigma(t)$ and $\ell(t)$ are the distances traveled across the detector and the solid phase, respectively. These distances are a function of time since the boundaries of the domain are moving (Fig. 2). The parameters μ_s and μ_d are the linear attenuation coefficients for the solid phase and the crystal in the detector, respectively. Unless there exists information on the distribution of attenuation coefficient μ_s in the domain, which could be provided, for example, by a scalar density field obtained by tomography, we assume that this attenuation coefficient is isotropic and constant along the path ds. We will come back to this aspect in Section 3.3. As regards attenuation coefficient μ_d, it is a specific property of

the detector. Its value depends on the energy of the photon detected, and data are available in [28].

A numerical approach based on a Monte-Carlo method can be used to compute almost exactly Eq. (2) [26]. This method consists of generating one thousand random photon histories in the direction of each detector and computing the corresponding distances ℓ and σ. For each direction, a specific weight function w_i corresponding to the solid angle is also computed, so that the efficiency is approximated as:

$$\xi_i(x,t) = \lim_{N\to\infty} \frac{1}{N}\sum_{i=1}^{N} w_i e^{-\mu_s \ell_i}(1 - e^{-\mu_d \sigma_i}), \tag{5}$$

which can also be viewed as the weighted solid angle along the photon history path. The precision of the approximation depends on the number N of photon histories computed. It has been found in previous studies [24,23] that one thousand is sufficient, which complies with the results obtained in this work.

2.4. Extension to systems with irregular moving boundaries

The problem is now to compute the value of $\ell(t)$, which requires computing the intersection point along the unit direction vector $\boldsymbol{\lambda} \in \mathbb{R}^3$ starting from $\mathbf{x}$ with the surface of the solid phase. With the existing technique, the intersection with the cylindrical boundary is computed by solving for $\ell \geq 0$:

$$x^2 + y^2 = r^2, \tag{6}$$

where $(x,y,z) = \ell\boldsymbol{\lambda} + \mathbf{x}$ and r is the radius of the cylindrical domain. Unfortunately, things are much more difficult in the case of a complex irregular boundary since there exists no simple expression such as Eq. (6) from which the value of can be obtained. The idea is to represent the domain V by a set of control nodes $\mathbf{P}_i \in V$ that forms an irregular tetrahedral mesh. The boundary $\partial V \subset V$ is represented by a surface tessellation using the nodes at the periphery of V. For any node $\mathbf{P}_i \in V$, the intersection with the surface mesh is computed for every random direction. This is a well known problem in computer science and the challenge here is to achieve the computation in a very efficient way. The intersection point $\mathbf{P}$ of a unit direction vector λ originating from $\mathbf{x}$ and a plane π_0 with a normal vector $\mathbf{n}$ and such that $\mathbf{P}_0 \in \pi_0$ can be found by solving:

$$(\mathbf{P} - \mathbf{P}_0)\cdot\mathbf{n} = 0. \tag{7}$$

Let us consider now a triangle T_n supported by three nodes $(\mathbf{P}_0,\mathbf{P}_1,\mathbf{P}_2) \in \partial V$ and the basis of vectors $\mathbf{b} = \{\mathbf{b}_1, \mathbf{b}_2, \mathbf{n}\}$ supporting this triangle with $\mathbf{b}_1 = \mathbf{P}_1 - \mathbf{P}_0$, $\mathbf{b}_2 = \mathbf{P}_2 - \mathbf{P}_0$ and $\mathbf{n} = \mathbf{b}_1 \times \mathbf{b}_2$. If $\mathbf{B} = [\mathbf{b}_1^T, \mathbf{b}_2^T, \mathbf{n}^T]^T$, the intersection point $\mathbf{P}$ can be then expressed as:

$$\mathbf{P} - \mathbf{P}_0 = \mathbf{k}\mathbf{B}. \tag{8}$$

For some vector $\mathbf{k} \in \mathbb{R}^3$, the necessary and sufficient conditions for having $\mathbf{P} \in T_n$ are that $\|\mathbf{k}\| \leq 1$ and $\mathbf{k} \in \mathbb{R}^3_+$ [29]. The value of $\ell(t)$ can then be calculated as $\ell = \|\mathbf{P} - \mathbf{x}\|$. In order to speed up the computations, a dynamic list using the tessellation can be constructed to determine the triangles that are more likely to intersect the photon path along the direction vector $\boldsymbol{\lambda}$. Indeed, for the same originating position, one thousand random directions pointing towards a given detector will necessarily be comprised within a certain region that contains a small subset of nodes of ∂V. In a first approximation, these nodes are assumed to be comprised within the volume of a cone with an opening angle α. A triangle is assumed to be part of this region if there exists at least one of its supporting nodes, $\mathbf{P}_i$, lying within this cone, or more precisely:

$$\boldsymbol{\delta}_i \cdot \boldsymbol{\lambda} \geq \cos\alpha, \tag{9}$$

where $\boldsymbol{\delta}_i$ is the unit vector starting from $\mathbf{x}$ and pointing towards $\mathbf{P}_i$. If for one random direction in particular, no such triangle can be found, every previously untested triangles are checked until at least one triangle satisfies the condition presented above. In order to increase the performance of the search algorithm, this triangle is then added to the list. In the case of a moving domain with fixed detectors, the relative position of the surface will change and affect the efficiency through changes in the traveled paths and the solid angle (Fig. 2). In order to account for specific domain kinematics, the time-dependent nodes are displaced accordingly by a combination of rotations and translations. The time step for the nodal displacement depends on the application. The photon histories and solid angles can be computed once for all and stored in files to generate a database for the reconstruction algorithm.

In the case of a system with moving boundaries, the presence of a gas–solid interface in the system has an impact on the efficiency since the linear attenuation of air is almost negligible with respect to that of glass. In fact, the computation ℓ of using the above procedure, which is the total length traveled across V, may lead, in some cases, to an overestimation of the attenuation integral of Eq. (4) and, as a result, to an inaccurate value of the efficiency. This is why the effect of the interface becomes stronger as the tracer approaches it or gets into the gas phase. This aspect will be discussed in Section 3.3.

2.5. Reconstruction of the tracer position

Prior to an experiment, the tracer is positioned in n specific positions $\{\mathbf{x}_k\}_{k=1..n}$ in order to calibrate the signal obtained by the discriminators (see Fig. 1). The activity of the source R, the dead-time of the detector τ and the attenuation coefficient of the solid phase μ_s are fitted by solving for each detector j:

$$\min_{R,\tau,\mu_s} \sum_{k=1}^{n} \left(\frac{\Phi_j(\mathbf{x}_k) - \Phi_j^m}{\Phi_j(\mathbf{x}_k) + \Phi_j^m} \right)^2, \tag{10}$$

where $\Phi_j(\mathbf{x}_k)$ is the number of events associated to position $\mathbf{x}_k$ and Φ_j^m is the measured value. Differences in the values of the source activity and detector dead-time are principally due to different settings of the amplifiers/discriminators. In the case of

μ_s, this may come from the anisotropy of the solid phase. For a given system, a dictionary of counts can then be generated and later used to associate to every node, through a model, a set of events that should be recorded by each detector (through the use of Eq. (1)). Next, given a set of event counts, the algorithm seeks the node $\mathbf{P}_i \in V$ such that:

$$\min_{\mathbf{P}_i \in V} \sum_{j=1}^{N} \left(\frac{\Phi_j^m - \Phi_j(\mathbf{P}_i)}{\Phi_j^m + \Phi_j(\mathbf{P}_i)} \right)^2 . \tag{11}$$

By using the mesh discretization, the algorithm further refines the seek by searching within every tetrahedron T_p containing the node $\mathbf{P}_i$ the position $\mathbf{x}_p$ that minimizes the error:

$$\min_{\mathbf{x}_p \in T_p} \sum_{j=1}^{N} \left(\frac{\Phi_j^m - \Phi_j(\mathbf{x}_p)}{\Phi_j^m + \Phi_j(\mathbf{x}_p)} \right)^2 . \tag{12}$$

The value of the counts at $\mathbf{x}_p$ is computed by linear interpolation using the values at the nodes of the corresponding tetrahedron.

3. Experimental

3.1. Material

The method introduced in the previous section was applied to a 16-qt Patterson–Kelley V-blender filled with 3-mm glass beads (2.5 kg/L), as presented in Fig. 3. The fill level was 40% in volume. The rotation of the blender was ensured by a DC motor coupled to a 50:1 gear reducer that drives the blender with a v strap in order to maintain a constant angular velocity. Eight 76 mm × 76 mm NaI (Tl) scintillation detectors (Teledyne Isotope S-1212-I) were fixed around the setup with aluminium rails. The saturation distance for every detector was determined when the counts indicated by the detector began to decrease as the source was moved away. Each of the detectors were connected to a scintillation tube and the signal was amplified by an ORTEC ACE Mate amplifier/discriminator (925-Scint). The dwell time for measurements was 7.0 ms.

The domain was decomposed with 46 404 tetrahedra and 13 067 nodes with a mesh size of 5 mm. The surface was approximated by 3634 triangles, which corresponds to a mesh size of 1.5 cm. To mimic the rotation of the domain, it was found that space steps of 5° were sufficient when using a second-order Lagrange polynomial for interpolation. The program for the dictionary generation was parallelized using the MPI communication library and was run on 8 AMD OPTERON 246 (2.0 GHz) processors of an IBM 64-processor cluster. The CPU-time required for the dictionary generation involving 72 angular positions and 8 detectors was 7.5 h. The reconstruction procedure for a 6 h experiment took approximately 30 min.

The isotope used for the tracer was scandium-46 with an activity of approximately 125 μCi, which emits gamma rays at 889 and 1120 keV. In the model, these two gamma rays are considered as two identical gamma rays with an average energy of 1005 keV. About 5 mg of scandium oxide was inserted into a glass bead and sealed by melting, which led to a perfectly spherical glass bead similar to those in the blender. The tracer was activated for 5 days using the SLOWPOKE nuclear reactor of Ecole Polytechnique. The tracer was used 5 days after its activation so that the sodium-24 isotope contained in the glass could decay. Traces of other isotopes were found to be negligible with respect to scandium-46.

3.2. Calibration

For calibration, the tracer was introduced at 12 axial positions in 6 aluminium probe ports located on the lids of the blender (Fig. 3). These ports are equally distributed in each tube of the V-blender, which allowed for the insertion of the Plexiglass rods to position the tracer during the calibration step. For each calibration position, events were recorded during 7.5 s. The rigid aluminium probe ports kept the Plexiglass rods from moving during the measurements. Eq. (10) was solved using the Fortran 90 CONMIN package for constrained optimization [30]. The relative error on the fit for each of the 72 calibration points was found to be Gaussian with a zero mean and 2.5% standard deviation, which indicates that the model can predict with rather good accuracy the experimental data.

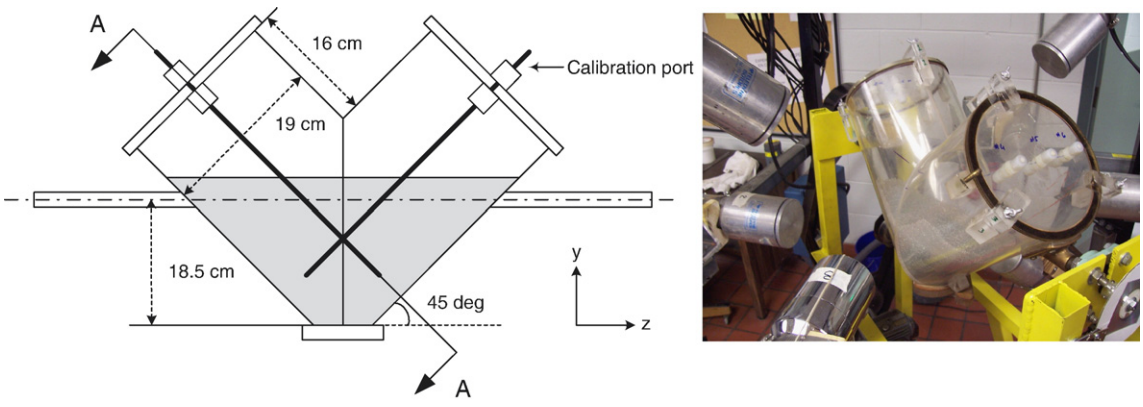

Fig. 3. Dimensions of the V-blender studied in this work.

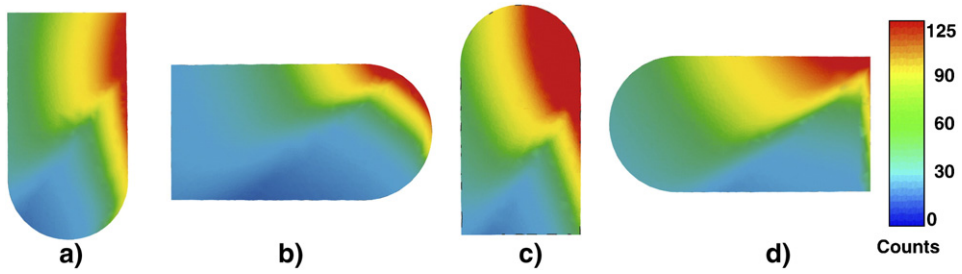

Fig. 4. Profile of event counts along the slice A–A of the V-blender from detector 1 showing the strong anisotropy induced by the interface: a) $\theta=0$, b)$\theta=\pi/2$, c)$\theta=\pi$, d)$\theta=3\pi/2$.

3.3. Effect of the interface

The presence of an interface in the system affects significantly the signal measured by the detectors. In fact, depending on the position of the tracer, more or less distance is traveled across the solid phase, thus affecting the attenuation in the sense of Beer–Lambert (see Fig. 2). This is why a good knowledge of the interface dynamics is required prior to any attempts for reconstruction.

The strategy employed to account for the presence of the interface comes from the calibration procedure. The surface is approximated by a free moving plane. Its position and orientation can be found by modifying the optimization problem of Eq. (10). In this work, two more variables were added, namely the angular orientation θ of the normal vector in the xy plane and the $y(t)$ coordinate of a point of the plane. More precisely, the problem to be solved takes the following form:

$$\min_{R,\tau,\mu_s,\theta,y_0} \sum_{k=1}^{n} \left(\frac{\Phi_j(\mathbf{x}_k) - \Phi_j^m}{\Phi_j(\mathbf{x}_k) + \Phi_j^m} \right)^2. \tag{13}$$

This corresponds to an indirect measure of the position of the interface by using the calibration procedure. In the case of the V-blender, it was observed that the plane orientation remains almost constant over time, the value of θ being close to that of the angle of repose of the powder ($\sim 30°$). As a result, θ can be determined once and for all using Eq. (13). The value of $y(t)$ obtained by solving the same problem is that at $t=0$, that is y_0. It was also observed that, during one revolution of the V-blender, this point moves translationally along the gravitational field (y axis). Its motion can then be described by means of the following expression:

$$y(t) = y_0 + a\sin^2\omega t, \tag{14}$$

where ω is the angular velocity of the blender (rad/s) and a is the amplitude of the periodic translational motion.

In order to illustrate the effect of the interface, a tracer was fixed at the end of one of the calibration ports (see Fig. 3) and submitted to 10 rotations with two different fill levels. When the blender is initially empty, there is no interference from the solid phase and the interface, which results in a smooth periodicity of the signal. When the blender is completely filled, the signal is slightly affected by the attenuation coming from the ray path across the solid phase to an extent that depends on the position of the tracer relative to the detector. In between these two limiting cases, the presence of an interface affects the number of events measured. This is illustrated in Fig. 4 that shows a profile of event counts along a slice A–A of the V-blender (see Fig. 3) for a fill level of 40%, over a complete revolution.

First, Fig. 5a shows the event counts with respect to the angular position of the V-blender when it is empty. It can be seen that the model can predict with very good accuracy the number of events recorded by a detector in this case. Since there

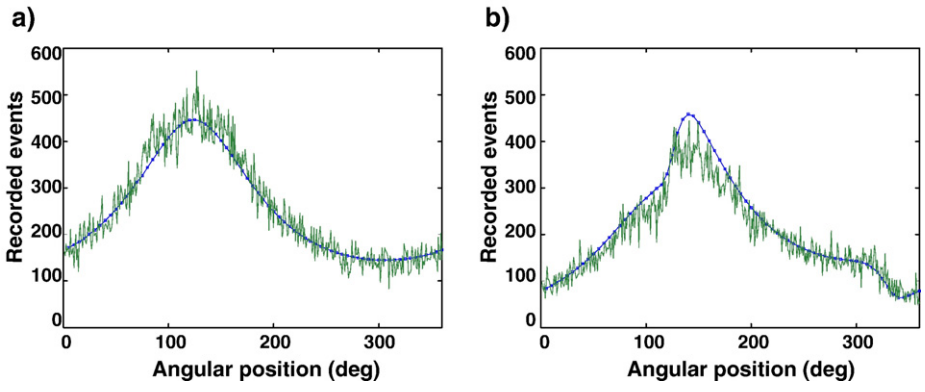

Fig. 5. Effect of the interface on the measured counts. The solid line represents the measured signal and the line with data points represents the model prediction for one detector. Results obtained for different fill levels: a) 0% b) 40%.

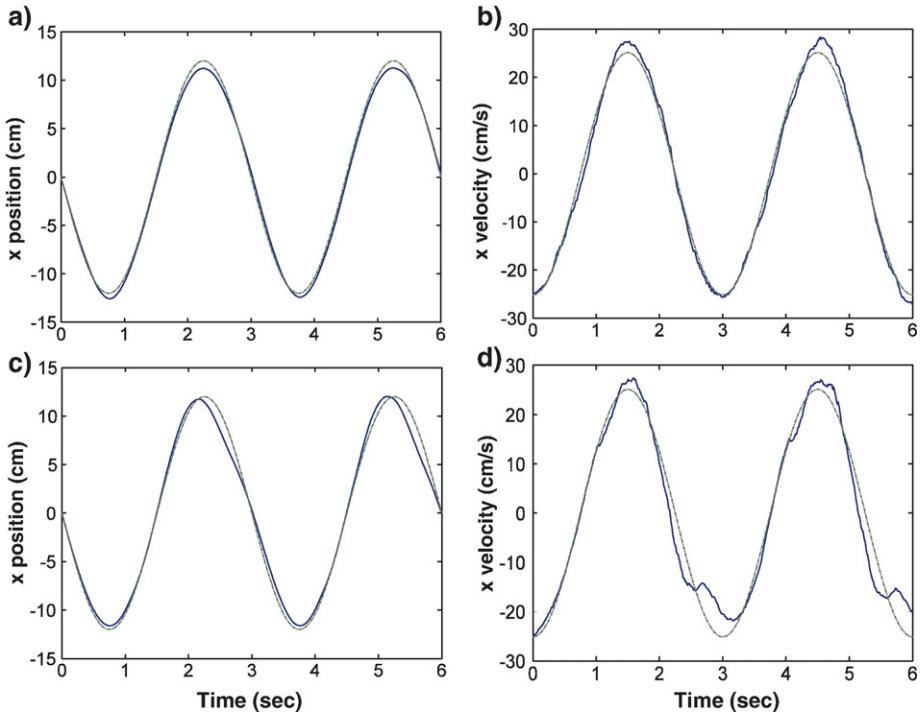

Fig. 6. Validation with a tracer in a fixed position in the empty V-blender at 20 rpm. The dashed line represents the expected position and the plain line is the map obtained. (a)–(b): the position (cm) and the velocity (cm/s) in the empty shell. (c)–(d): the position (cm) and the velocity (cm/s) in a 40% filled shell.

is no attenuation for a 0% fill level, this indicates that the variation of the solid angle resulting from the motion of the tracer is well taken into account by the proposed RPT technique. Next, it can be seen in Fig. 5b that corresponds to a 40% fill level, that the solid phase and the position of the interface influence the attenuation, which results in non-negligible interactions between the photons and the particles and a reduction of the signal measured, especially around an angular position of 150°. Consequently, in order to position with good accuracy the tracer in the domain, the model must be able to predict the position of this interface. It can be concluded from results of Fig. 5 that the proposed approach is robust and suitable for predicting the number of events recorded by a detector from any position of the tracer in the domain.

The proposed RPT technique is based on a priori knowledge of the shape and dynamics of the interface in the domain. In the case of the V-blender, three parameters (y_0,θ,a) were used for this purpose. This approach could be extended to other blenders or geometries, but might require more sophisticated models relying on more parameters for describing the motion of the interface. It also makes no doubt that the particle density data coming for instance from tomography imaging technology could facilitate the derivation of such models.

4. Results and discussion

4.1. Validation

The extended RPT technique was validated in four different cases. First, the position of a free flowing tracer was reconstructed in a fluidized bed and compared to the results obtained with the original RPT technique. The maps obtained were similar and slight discrepancies between the solutions can be explained by the fact that different convergence criteria and parameters for the constrained optimization algorithm were used. Next, the position of 72 motionless calibration points along rods inserted in the six calibration ports of the V-blender was predicted with very good accuracy. The third case consisted in placing the tracer in a fixed position in one of the calibration ports and initiating the rotation of the shell. In order to assess the effect of the shape of the geometry with no regards to the position of the interface, the V-blender was filled at 0%and 100%. Maps were then obtained for different angular velocities between 20 and 60 rpm. A typical result at 20 rpm is presented in Fig. 6a and b, which show the x-component of the position and velocity field with respect to the time in the empty V-blender. As can be seen, the agreement between the expected position and the predicted map is very good. It can be observed that the largest discrepancies between the expected position and the predicted map are smaller than 10%, which results in an error of less than 15% for the velocity. Similar results were obtained for y- and z-components. No loss of precision was detected at higher angular velocities.

The fourth validation is similar to the third except that the blender was 40 filled in order to mimic realistic experimental conditions. In this case, the effect of the interface plays a major role, the tracer going back and forth through this interface during a complete revolution. The corresponding results presented in Fig. 6c and d also show a good agreement between the expected position and the predicted map, and the error is

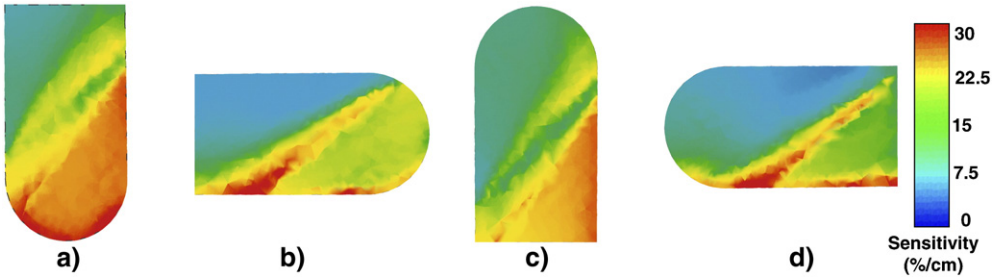

Fig. 7. Profile of sensitivity S_T (%/cm^{-1}) along the slice A–A of the V-blender: a) $\theta=0$, b) $\theta=\pi/2$, c)$\theta=\pi$, d)$\theta=3\pi/2$.

slightly larger than that in the case of the empty shell. This holds especially when the tracer goes back into the solid phase, that is, after around 2.5 s and 5.5 s. This is undoubtedly due to the interface, which affects the signal measured by the detectors. Another source of error is the assumption of a flat plane for the interface, which is an approximation of its real shape. One must however realize that the third and fourth cases are extreme cases since, in practical situations, the tracer will not be maintained fixed in the domain, but will rather flow with the bulk of inert particles. For the sake of completeness and to better understand why the largest errors occur when the tracer is not in the solid phase, a sensitivity analysis, as carried out by Godfroy et al. [23], is now presented.

4.2. Sensitivity analysis

The theoretical sensitivity S with respect to x can be computed by:

$$S(x) = \frac{1}{\Phi}\frac{\partial \Phi}{\partial x} = \frac{\partial \ln \Phi}{\partial x}. \tag{15}$$

It represents the change in recorded events when the tracer undergoes a small displacement dx. Following the work of Roy et al. [22], in the case of a multiple detector arrangement, the overall sensitivity S_T is given by:

$$S_T^2(x) = \sum_{i=1}^{n} \left(\frac{\partial \ln \Phi_i}{\partial x}\right)^2, \tag{16}$$

where n is the number of detectors. Also, the resolution $R(x)$ of a map is given by:

$$R(x) = \frac{1}{S(x)\sqrt{\Phi}}. \tag{17}$$

This value is related to the accuracy of reconstruction. This means that the larger the sensitivity along the path, or the smaller the number of counts Φ, the better the resolution. Fig. 7 shows the profile of S_T along the slice A–A of the V-blender. As can be seen, the sensitivity is smaller when the tracer is not in the solid phase. It is then expected that the map resolution $R(x)$ will be larger in such a case. It can be concluded that the accuracy of the reconstruction will be better when the tracer is in the solid part, a situation that is likely to occur in practice.

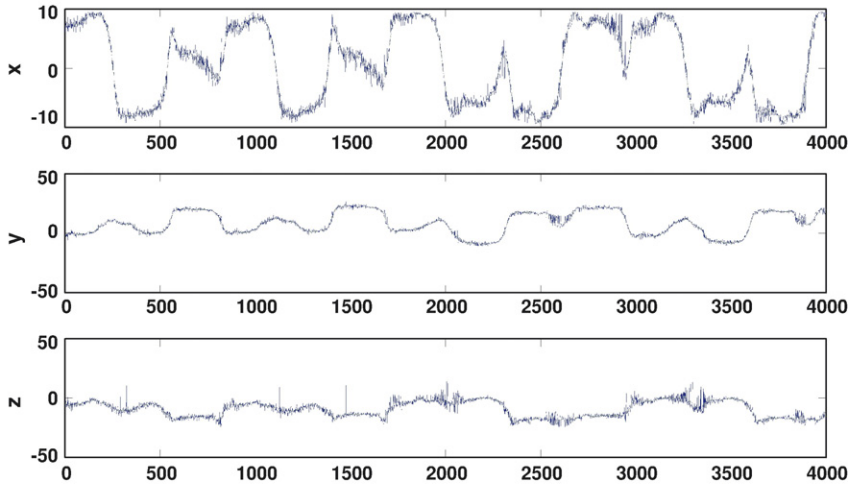

Fig. 8. Typical signal obtained from the inverse map function showing the x, y, and z components of the tracer position during 4096 samplings with a dwell time of 7 ms.

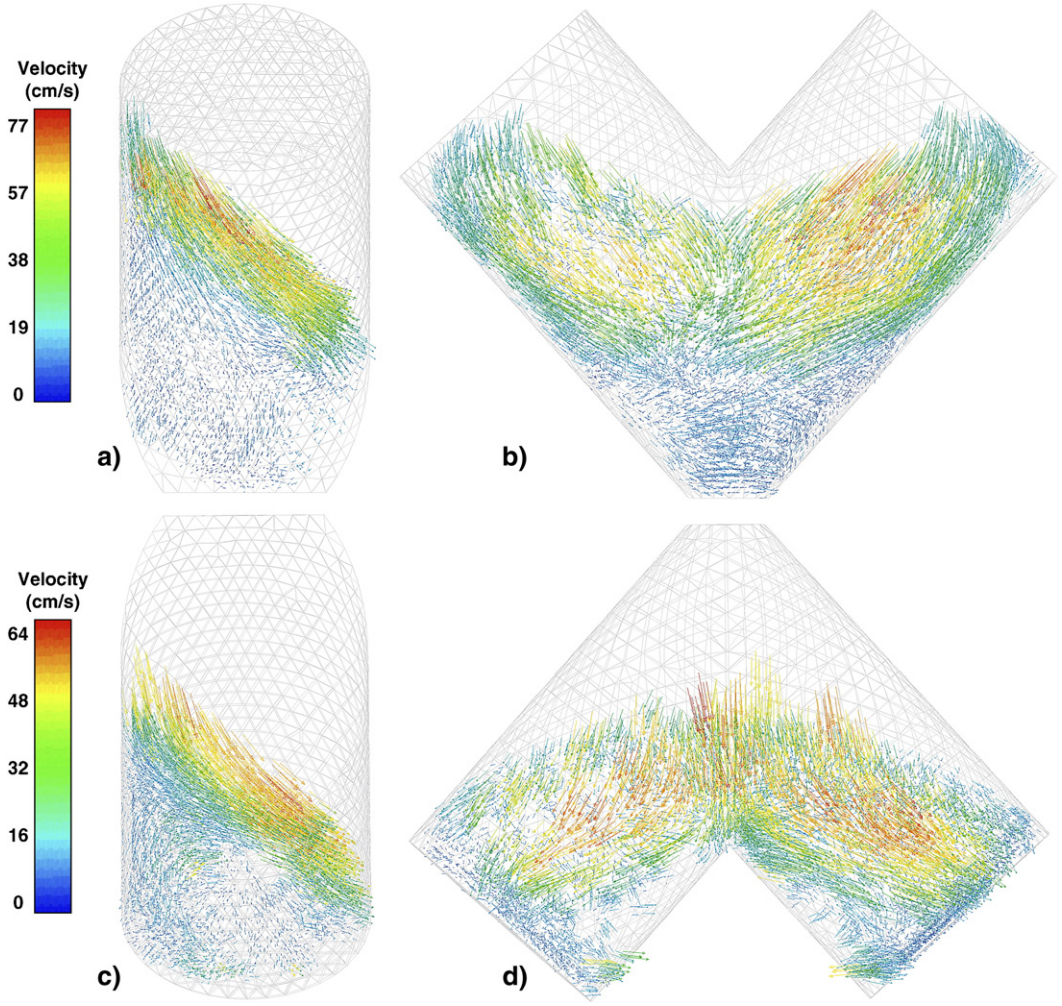

Fig. 9. Typical mean velocity field obtained after reconstruction. (a)–(b): Angular position $\theta \in [0°,5°]$ (cm/s). (c)–(d): Angular position $\theta \in [177\ 5°,182\ 5°]$ (cm/s).

4.3. Mean velocity field

The mean velocity field can be obtained from the RPT raw signal by averaging the velocity of the tracer over the entire set of elements forming the domain. Such a typical raw signal is presented in Fig. 8.

For each time step, the tracer was located in the mesh and its velocity was stored in a data structure at a position given by the corresponding element number. For each element, the mean velocity was obtained at the end by dividing the sum of the velocities recorded by the number of occurrences of the tracer in this element. A coarser mesh was considered for these calculations in order to increase the occurrences of the tracer per element.

Fig. 9 displays the mean velocity field at different angular positions. It represents the averaged velocity within an angular span of 5°. In particular, an avalanche of particles at the interface is clearly visible in Fig. 9a and c, these particles flowing at relatively high speed. A closer look at Fig. 9 reveals that, even though the interface was assumed to be flat in the calculations, its position and shape was predicted with reasonable accuracy. As can be seen on the figure, the interface is the combination of two planes that join along the axis of symmetry of the V-blender. One explanation could be related to the fact that, when solving the minimization problems of Eqs. (11) and (12), more weight is given to the detectors with a low number of counts. For example, when the tracer is close to the interface, more weight is given to the detectors behind it since the distance traveled in the solid part is then longer, which results in a low number of counts for these detectors. Consequently, since the signal measured in this case is less affected by the shape and the position of the interface, the error resulting from the use of an approximation for this interface is small.

5. Conclusion

An extended RPT method was developed by proposing an original method to solve the inverse map problem in the case of systems with irregular moving boundaries. This generalized method, which is based on an existing Monte-Carlo method [24], relies on an irregular mesh of cells to represent the geometry of the domain. This approach enables, in principle, the study of systems of any shape and any kinematics (e.g. tote

blenders, V-blenders) through a complete map of the flow field including a set of Lagrangian trajectories.

The novel RPT method was first presented in detail. Four different validations (the first one in a fluidized bed and the other ones in a Patterson–Kelley 16-qt V-blender) were performed under different operating conditions in order to assess the robustness and the reliability of this RPT technique. A sensitivity analysis was also carried out, which served to explain the effect of the interface on the accuracy of the method. The method was then successfully applied to generate a mean Eulerian velocity profile in a V-blender.

A different calibration procedure, which would consist of calibrating at different angular positions of the shell, might improve the RPT method developed in this work. Moreover, an optimal positioning of the detectors around the system might significantly help to improve the resolution [22]. Finally, positioning the interface accurately during the motion of the domain is an important aspect of the method. Better ways to position this interface could be envisaged by resorting, for instance, to tomography imaging technology.

Acknowledgements

The authors are grateful to R. Mabrouk for his help and support, and also to Dr. Greg Kennedy from the Institute of Nuclear Engineering for the activation of the tracer. The authors would like to thank the Research and Development Center of ratiopharm operations (Mirabel, Québec) and its Vice President R&D Dr A. Ouali, and NSERC for providing financial support for this work.

References

[1] F. Bertrand, L.-A. Leclaire, G. Levecque, DEM-based models for the mixing of granular materials, Chemical Engineering Science 60 (2005) 2517–2531.
[2] F.J. Muzzio, C.L. Goodridge, A. Alexander, P. Arratia, H. Yang, O. Sudah, G. Mergen, Sampling and characterization of pharmaceutical powders and granular blends, International Journal of Pharmaceutics 250 (2003) 51–64.
[3] D.A. Steingart, J.W. Evans, Measurements of granular flows in two-dimensional hoppers by particle image velocimetry. Part I: experimental method and results, Chemical Engineering Science 60 (2005) 1043–1051.
[4] M.R. Hawkesworth, D.J. Parker, P. Fowles, J.F. Crilly, N.I. Jefferies, G. Jonkers, Nonmedical applications of a positron camera, Nuclear Instruments & Methods in Physics Research. Section A, Accelerators, Spectrometers, Detectors and Associated Equipment 310 (1–2) (1991) 423–434.
[5] J.S. Lin, M.M. Chen, B.T. Chao, A novel radioactive particle tracking facility for measurement of solids motion in gas fluidized beds, AIChE Journal 31 (3) (1985) 465–473.
[6] S. Degaleesan, M.P. Dudukovic, Y. Pan, Application of wavelet filtering to the radioactive particle tracking technique, Flow Measurement and Instrumentation 13 (1–2) (2002) 31–43.
[7] S. Limtrakul, J. Chen, P.A. Ramachandran, M.P. Dudukovic, Solids motion and holdup profiles in liquid fluidized beds, Chemical Engineering Science 60 (7) (2005) 1889–1900.
[8] F. Larachi, J. Chaouki, G. Kennedy, 3-D mapping of solids flow fields in multiphase reactors with RPT, AIChE Journal 41 (2) (1995) 439–443.
[9] F. Larachi, M. Cassanello, M. Marie, J. Chaouki, C. Guy, Solids circulation patterns in three-phase fluidized beds containing binary mixtures of particles as inferred from RPT, Chemical Engineering Research and Design, Transactions of the Institute of Chemical Engineers, Part A 73 (A3) (1995) 263–268.
[10] M. Cassanello, F. Larachi, C. Guy, J. Chaouki, Solids mixing in gas–liquid–solid fluidized beds: experiments and modeling, Chemical Engineering Science 51 (10 pt A) (1996) 2011–2020.
[11] F. Larachi, B.P.A. Grandjean, J. Chaouki, Mixing and circulation of solids in spouted beds: particle tracking and Monte Carlo emulation of the gross flow pattern, Chemical Engineering Science 58 (8) (2003).
[12] G.M. Field, J. Bridgwater, T.D. Beynon, J.S.M. Botterill, Mechanics of powder mixing using positron emission tomography, Nuclear Instruments & Methods in Physics Research. Section A, Accelerators, Spectrometers, Detectors and Associated Equipment 310 (1–2) (1991) 435.
[13] C.J. Broadbent, J. Bridgwater, D.J. Parker, S.T. Keningley, P. Knight, Phenomenological study of a batch mixer using a positron camera, Powder Technology 76 (3) (1993) 317–329.
[14] J.R. Jones, J. Bridgwater, Case study of particle mixing in a ploughshare mixer using positron emission particle tracking, International Journal of Mineral Processing 53 (1–2) (1998) 29–38.
[15] S. Forrest, J. Bridgwater, P.R. Mort, J. Litster, D.J. Parker, Flow patterns in granulating systems, Powder Technology 130 (1–3) (2003) 91–96.
[16] M.J.P. Hiseman, B.F.C. Laurent, J. Bridgwater, D.I. Wilson, D.J. Parker, N. North, D.R. Merrifield, Granular flow in a planetary mixer, Chemical Engineering Research & Design 80 (5) (2002) 432–440.
[17] B. Laurent, J. Bridgwater, Continuous mixing of solids, Chemical Engineering & Technology 23 (1) (2000) 16–18.
[18] H.P. Kuo, P.C. Knight, D.J. Parker, M.J. Adams, J.P.K. Seville, Discrete element simulations of a high-shear mixer, Advanced Powder Technology 15 (3) (2004) 297–309.
[19] H.P. Kuo, P.C. Knight, D.J. Parker, J.P.K. Seville, Solids circulation and axial dispersion of cohesionless particles in a V-mixer, Powder Technology 152 (2005) 133–140.
[20] M. Cassanello, F. Larachi, M.-N. Marie, C. Guy, J. Chaouki, Experimental characterization of the solid phase chaotic dynamics in three-phase fluidization, Industrial & Engineering Chemistry Research 34 (9) (1995) 2971–2980.
[21] F. Larachi, M. Cassanello, J. Chaouki, C. Guy, Flow structure of the solids in a 3-D gas–liquid–solid fluidized bed, AIChE Journal 42 (9) (1996) 2439–2452.
[22] S. Roy, F. Larachi, M.H. Al-Dahhana, M.P. Dudukovic, Optimal design of radioactive particle tracking experiments for flow mapping in opaque multiphase reactors, Applied Radiation and Isotopes 56 (2002) 485–503.
[23] L. Godfroy, F. Larachi, G. Kennedy, B. Grandjean, J. Chaouki, On-line flow visualization in multiphase reactors using neural networks, Applied Radiation and Isotopes 48 (2) (1997) 225–235.
[24] F. Larachi, G. Kennedy, J. Chaouki, Gamma-ray detection system for 3-D particle tracking in multiphase reactors, Nuclear Instruments & Methods in Physics Research. Section A, Accelerators, Spectrometers, Detectors and Associated Equipment A338 (2–3) (1994) 568–576.
[25] R.G. Sherritt, J. Chaouki, A.K. Mehrotra, L.A. Behie, Axial dispersion in the three-dimensional mixing of particles in a rotating drum reactor, Chemical Engineering Science 58 (2) (2003) 401–415.
[26] G.B. Beam, L. Wielopolski, R.P. Gardner, K. Verghese, Monte Carlo calculation of efficiencies of right-circular cylindrical NaI detectors for arbitrarily located point sources, Nuclear Instruments and Methods 154 (3) (1978) 501–508.
[27] G.F. Knoll, Radiation Detection and Measurement, 3rd edition, John Wiley and Sons, 2000.
[28] B.J. Snyder, G.L. Gyorey, Calculating gamma efficiencies in scintillation detectors, Nucleonics 23 (1965) 80–86.
[29] G. Dhatt, G. Touzot, The Finite Element Method Displayed, John Wiley and Sons, New York, 1984.
[30] G.N. Vanderplaats, CONMIN User's manual. NASA technical memorandum X-62282, NASA, 1978.